13PFL-0819

Li-Ion Battery SoC Estimation Using a Bayesian Tracker

Author, co-author (Do NOT enter this information. It will be pulled from participant tab in MyTechZone)

Affiliation (Do NOT enter this information. It will be pulled from participant tab in MyTechZone)

ABSTRACT

Hybrid, plug-in hybrid, and electric vehicles have enthusiastically embraced rechargeable Li-ion batteries as their primary/supplemental power source of choice. Because the state of charge (SoC) of a battery indicates available remaining energy, the battery management system of these vehicles must estimate the SoC accurately. To estimate the SoC of Li-ion batteries, we derive a normalized state-space model based on Li-ion electrochemistry and apply a Bayesian algorithm. The Bayesian algorithm is obtained by modifying Potter's square-root filter and named the Potter SoC tracker (PST) in this paper. We test the PST in challenging test cases including high-rate charge/discharge cycles with outlier cell voltage measurements. The simulation results reveal that the PST can estimate the SoC with accuracy above 95% without experiencing divergence.

INTRODUCTION

Recently, hybrid and electric vehicles have received substantial attention due to their high fuel efficiency, low cost of operation and reduced greenhouse gas emission. At the heart of these vehicles lies rechargeable (secondary) batteries as a source of energy. Specifically, Li-ion batteries have become a more popular choice than NiMH batteries in newer generation hybrid and electric vehicles due to their high energy density, slow self-discharge, and zero memory effect. A battery management system (BMS) is required to keep the Li-ion cells within their specified operating range by sensing voltage, current, temperature and internal pressure signals. This ensures the availability of reliable electrical power, improves overall energy efficiency, protects cells from damage and prolongs battery lifespan. The battery SoC is one of the most important parameters that BMS estimates in real time to accomplish its goals. The SoC needs to be estimated accurately in a broad range of environmental and operating conditions, including environmental temperature (from freezing cold to scorching hot) and battery age (from new to old). To this end, the following two key elements must be readily available:

- An accurate battery model and
- A robust SoC estimation strategy.

A Brief Review of Battery Modelling

Modeling refers to the process of analysis and synthesis to determine a suitable mathematical description that characterizes the relevant dynamics of a component under test. To be useful, the model must be scalable and easy to be simulated. A battery model is required to capture battery physics accurately. The two broad approaches to battery modelling are

- Equivalent electrical-circuit modeling and
- Electrochemical modeling

Equivalent electrical-circuit models use RC (Resistor-Capacitor) circuits to model the charge and discharge behavior of Li-ion batteries [15, 24, 10]. They may consist of the first-order, second-order or the third-order RC models coupled with a hysteresis effect [24, 10]. Equivalent circuit models are conceptually simple to understand and use a few parameters to be identified. However, they provide little insight into underlying physical battery limitations. On the other hand, electrochemical modeling uses the first principles– they use partial differential equations to capture the diffusion dynamics of Li-ions in the solid phase composite electrodes and the electrolyte. Although electrochemical modeling provides a more accurate SoC estimate, it comes with a price; it requires many unknown parameters to be identified. However, once an electrochemical model is developed, it can be easily manipulated to meet different battery specifications. For these reasons, electrochemical modeling is often preferred to equivalent electrical-circuit modeling [17, 7].

A Brief Review of SoC Estimation methods

Estimating the SoC in an electric vehicle is analogous to gauging fuel in a conventional vehicle. In general, SoC estimation techniques can be broadly categorized into two types:

- Direct techniques

- Indirect techniques

The most widely used direct technique is called *Coulomb counting* [6]. Coulomb counting relies on integrating all battery charge and discharge currents. If the initial battery capacity is known and the coulometric efficiency is 100%, it will estimate the SoC accurately. However, in practice, all the charge current are not used for increasing the battery capacity. By the same token, battery capacity losses cannot be attributed to external discharge current only. For this reason, Coulomb counting is unreliable for hybrid electric vehicle applications.

On the other hand, in indirect methods, the SoC is estimated based on some battery physical parameters such as the open-circuit/terminal voltage or the battery acid concentration [4, 13, 14]. Indirect methods can be used to estimate the SoC accurately in a wide range of operating conditions. For example, in *impedance spectroscopy*, the battery impedance is measured through frequency variations. Unfortunately, this technique can be implemented only in a laboratory setting because it requires additional signals. Another widely used indirect technique is rooted in *Bayesian estimation theory*. The extended Kalman filter (EKF) is one of the most widely used suboptimal Bayesian estimators for estimating the battery SoC from the battery voltage measurements [7, 26, 18]. Although the EKF can estimate the SoC accurately, it will be bound to fail if it is not initialized properly or the noise parameters do not sufficiently account for various model mismatches.

The main motivation of this paper has been to estimate the SoC accurately in a wide range of challenging applications. To this end, we make the following two contributions for the first time ever in the battery literature:

- *Formulating a Normalized State-Space Model for Cell Chemistry*. The electrochemical model uses a set of coupled non-linear partial differential equations to capture the diffusion dynamics of Li-ions in the solid-phase electrodes. For computational reasons, during estimation, the diffusion model is reduced to have a relatively less order and normalized with respect to maximum solid-phase Li-ion concentration. The resulting normalized electrochemical state-space model has been useful for us to set up various parameters related to a SoC estimator.
- *Developing an Algorithm for SoC Tracking*. This paper proposes a modified version of Potter's square-root algorithm [12] and the resulting algorithm is named the Potter SoC Tracker (PST). A square-root formulation of the PST promotes the stability when committed to limited-precision micro controllers.

The rest of the paper is organized as follows: The next section presents the electrochemical modeling of Li-ion batteries and relates it with a state-space model for Bayesian estimation. Then, we go on to derive the PST algorithm. After that, the PST is tested for SoC estimation in various challenging scenarios. Finally, the paper concludes with some remarks.

ELECTROCHEMICAL MODELING

As shown in Fig. 1, a Li-ion electrochemical cell has three main domains– two composite electrodes (positive and negative) and a separator. According to porous electrode theory developed by Newman and Tiedemann [16], composite electrodes are modeled using porous electrode theory. Porous electrode theory treats the solid and electrolyte phases as superimposed continua without regard to microstructure. Composite electrodes provide large interfaces between electrode and electrolyte resulting in a fast electrochemical reaction. Doyle *et al.* [8, 11] were the first to model a Li-ion cell by combining porous elcectrode theory with concentrated solution theory. In Li-ion cells, the active material of the negative electrode is typically a crystalline material, such as graphite whereas it is a transition-metal oxide such as NiO_2, CoO_2 and Mn_2O_4 in the positive electrode. Li-ions are shuttled between positive and negative electrodes during cell charge and discharge events.

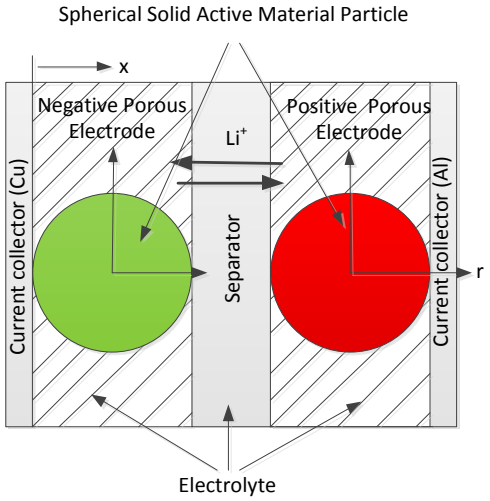

Figure 1: ***One Dimensional (x-direction) Electrochemical Cell Model Coupled with Solid Particle Diffusion Submodel (r-direction)***

For Li-ion cells, the one-dimensional electrochemical model captures relevant solid and electrolyte phase diffusion dynamics and accurately predicts current/voltgae response. In this paper, the dimension-of-interest is the horizontal (x-) axis (see Fig. 1). Moreover, throughout this paper, we follow the following convention: the subscripts s, e and se are used to refer to the solid particle, electrolyte and solid-electrolyte interface, respectively; the subscripts p and n are used to denote the quantities related to the positive and negative electrodes, respectively. If the electrolyte concentration gradient is constant and cell parameters listed in Table I are constant, Li-ion chemistry boils down to a solid (particle) phase diffusion equation governed by Fick's

second law:

$$\dot{c}_s = \frac{\partial c_s}{\partial t} = D_s\Big[\frac{\partial^2 c_s}{\partial r^2} + \frac{2}{r}\frac{\partial c_s}{\partial r}\Big], \quad (1)$$

with a couple of boundary conditions

$$\frac{\partial c_s}{\partial r}|_{r=0} = 0 \quad (2)$$

$$-D_s\frac{\partial c_s}{\partial r}|_{r=R_s} = \frac{J^{Li}}{Fa_s}, \quad (3)$$

where $c_s(r,t)$ is the Li-ion concentration in the solid phase and the second boundary condition (3) is due to Fick's first law of diffusion.

The Butler-Volmer current density, J^{Li}, in (3) is a measure of reaction rate and coupled to the electrode overpotential η by the following Butler-Volmer kinetic expression:

$$J^{Li} = a_s j_0\Big[\exp\big(\frac{\alpha_a F}{RT}\eta\big) - \exp\big(\frac{\alpha_c F}{RT}\eta\big)\Big], \quad (4)$$

where R and T refer to the universal gas constant and temperature in K, respectively, and the exchange current density

$$j_0 = (c_e)^{\alpha_a}(c_{s,max} - c_{se})^{\alpha_a}(c_{se})^{\alpha_c}.$$

The overpotential, η, is the difference between the solid and electrolyte potentials minus the open circuit potential of the solid or $\eta = \phi_s - \phi_e - U$.

Note that the assumptions to obtain the electrochemical model (1)-(3) can be readily relaxed at the cost of a more sophisticated model. In what follows, the electrochemical model is converted to a state-space model, which consists of a couple of equations, namely, the state equation and the measurement equation.

Deriving the State Equation

Standard estimation and control methods require a dynamic model expressed as a low-order set of ordinary differential equations, which is often referred to as the state/process equation of a state-space model. For this reason, as a first step in electrochemical modeling, the set of partial differential equations present in (1)-(3) needs to be converted to a set of ordinary differential equations. In this subsection, we use finite difference approximation [21, 7]. Assume that the spherical electrode particle is divided into N_r shells, each of which has a thickness of

$$\Delta r = \frac{R_s}{N_r}$$

and a radius of $r_i = i\Delta r$, where $i = 1, 2 \dots N_r$. Applying the following two finite difference approximations

$$\frac{\partial c_s}{\partial r} = \lim_{\Delta r\to 0}\frac{c_{s_{i+1}} - c_{s_{i-1}}}{2\Delta r} \quad (5)$$

$$\frac{\partial^2 c_s}{\partial r^2} = \lim_{\Delta r\to 0}\frac{c_{s_{i+1}} - 2c_{s_i} + c_{s_{i-1}}}{\Delta r^2} \quad (6)$$

to (1) yields ($i = 1, 2 \dots (N_r - 1)$)

$$\dot{c}_{s_i} = \frac{D_s}{\Delta r^2}\big[\frac{i+1}{i}c_{s_{i+1}} - 2c_{s_i} + \frac{i-1}{i}c_{s_{i-1}}\big] \quad (7)$$

Applying the finite difference approximation to the boundary condition in (3), we get

$$c_{s_{N_r}} = c_{s_{N_r-1}} - \frac{\Delta r}{Fa_s D_s}J^{Li}. \quad (8)$$

Substituting (8) into (7) when $i = (N_r - 1)$ yields

$$\dot{c}_{s_{N_r-1}} = \frac{D_s}{\Delta r^2}\Big[\Big(\frac{N_r-2}{N_r-1}\Big)c_{s_{N_r-2}} - \Big(\frac{N_r-2}{N_r-1}\Big)c_{s_{N_r-1}} + \frac{\Delta r}{Fa_s D_s}\Big(\frac{N_r}{N_r-1}\Big)J^{Li}\Big]. \quad (9)$$

Combining (7) and (9) into a matrix form, we get the following linear time-invariant state equation in continuous-time:

$$\dot{\mathbf{c}}_s = \mathbf{A}\mathbf{c}_s + \mathbf{B}J^{Li}, \quad (10)$$

where the $(N_r - 1)$-dimensional concentration state vector

$$\mathbf{c}_s = [c_{s_1}\ c_{s_2} \dots c_{s_{N_r-1}}]^T$$

$$\mathbf{A} = \frac{D_s}{\Delta r^2}\begin{pmatrix} -2 & 2 & 0 & 0 & \dots & 0 \\ 1/2 & -2 & 3/2 & 0 & \dots & 0 \\ \vdots & \vdots & \vdots & \vdots & \vdots & \vdots \\ 0 & 0 & \dots & \frac{N_r-3}{N_r-2} & -2 & \frac{N_r-1}{N_r-2} \\ 0 & 0 & 0 & \dots & \frac{N_r-2}{N_r-1} & -\frac{N_r-2}{N_r-1} \end{pmatrix}$$

$$\mathbf{B} = \frac{-1}{Fa_s\Delta r}\big[0\ \ 0 \dots 0\ \ \frac{N_r}{(N_r-1)}\big]^T$$

For a constant diffusion coefficient D_s, the matrix $\mathbf{A}$ becomes constant and tri-diagonal.

Deriving the Measurement Equation

In this subsection, the second equation of the electrochemical state-space model, known as the measurement equation, is derived. The input to the model is the charge/discharge current, I, applied to the battery and the output is the corresponding battery terminal voltage, V. The battery voltage is determined by the equation [7]:

$$V = \phi_{s,p} - \phi_{s,n} - R_f I, \quad (11)$$

where the solid phase potentials of the positive and negative electrodes are defined, respectively, as follows:

$$\phi_{s,p} = \eta_p + \phi_{e,p} + U_p(\varphi_{se,p}) \quad (12)$$

$$\phi_{s,n} = \eta_n + \phi_{e,n} + U_n(\varphi_{se,n}) \quad (13)$$

Here, η denotes the over-potential and U denotes the open circuit potentials also known as local equilibrium potentials. Substituting (12)-(13) into (11), we get

$$V = \eta_p + \phi_{e,p} + U_p(\varphi_{se,p}) - \eta_n - \phi_{e,n} - U_n(\varphi_{se,n}) - R_f I. \quad (14)$$

Grouping alike terms on the right hand side of (14) together yields

$$V = (\eta_p - \eta_n) + (\phi_{e,p} - \phi_{e,n}) + (U_p(c_{se,p}) - U_n(c_{se,n})) - R_f I. \quad (15)$$

The first three terms on the right hand side of (15) are given as follows:

- The overpotentials of the positive and negative electrodes can be calculated, as shown by:

$$\eta_p = \frac{RT}{\alpha_a F}\ln(\xi_p + \sqrt{\xi_p^2+1})$$
$$\eta_n = \frac{RT}{\alpha_a F}\ln(\xi_n + \sqrt{\xi_n^2+1}),$$

where

$$\xi_p = \frac{J_p^{Li}}{2a_s j_{0,p}}$$
$$\xi_n = \frac{J_n^{Li}}{2a_s j_{0,n}},$$

where the exchange current densities

$$j_{0,p} = (c_e)^{\alpha_a}(c_{s,max,p} - c_{se,p})^{\alpha_a}(c_{se,p})^{\alpha_c}$$
$$j_{0,n} = (c_e)^{\alpha_a}(c_{s,max,n} - c_{se,n})^{\alpha_a}(c_{se,n})^{\alpha_c}.$$

The Butler-Volmer current densities at the positive and negative electrodes, J_p^{Li} and J_n^{Li}, are defined as follows:

$$J_p^{Li} = a_s j_{0,p}\Big[\exp\big(\frac{\alpha_a F}{RT}\eta_p\big) - \exp\big(\frac{\alpha_c F}{RT}\eta_p\big)\Big]$$
$$J_n^{Li} = a_s j_{0,n}\Big[\exp\big(\frac{\alpha_a F}{RT}\eta_n\big) - \exp\big(\frac{\alpha_c F}{RT}\eta_n\big)\Big].$$

Assuming that the Butler-Volmer current is constant along the x-axis, the approximate value for J_p^{Li} can be found as follows:

$$\int_0^{\delta_p} J_p^{Li}dx = \frac{-I}{A} \Rightarrow J_p^{Li} \simeq -\frac{I}{A\delta_p}. \quad (16)$$

Similarly, we obtain

$$J_n^{Li} \simeq \frac{I}{A\delta_n}. \quad (17)$$

- The open circuit potential (OCP) refers to the voltage between the battery terminals when no load is applied and the battery is completely relaxed. The OCP depends on the SoC (or the solid phase concentration) and increases with the SoC. The OCP is empirically determined– The OCP at a specific SoC is determined by averaging the battery terminal voltage observed at that SoC during charging and discharging. In this paper, the following two empirical equations are used for simulation [7]:

$$\begin{aligned} U_p(\varphi_{se,p}) &= 85.681\varphi_{se,p}^6 - 357.7\varphi_{se,p}^5 \\ &\quad +613.89\varphi_{se,p}^4 - 555.65\varphi_{se,p}^3 \\ &\quad +281.06\varphi_{se,p}^2 - 76.648\varphi_{se,p} \\ &\quad +13.1983 - 0.30987\exp(5.657\varphi_{se,p}^{115}) \\ U_n(\varphi_{se,n}) &= 8.0029 + 5.064\varphi_{se,n} - 12.578\varphi_{se,n}^{0.5} \\ &\quad -(8.6322\times10^{-4}\varphi_{se,n}^{-1}) \\ &\quad +(2.176\times10^{-5}\varphi_{se,n}^{1.5}) \\ &\quad -0.46016\exp(15(0.06-\varphi_{se,n})) \\ &\quad -0.55364\exp(-2.4326(\varphi_{se,n}-0.92)), \end{aligned}$$

where the normalized concentration at the solid-electrolyte interface of the positive electrode, $\varphi_{se,p}$, is given by

$$\varphi_{se,p} = \frac{\text{Concentration at Solid-Electrolyte Interface}}{\text{Maximum Solid Phase Concentration}} = \frac{c_{se,p}}{c_{s,max,p}}. \quad (18)$$

The term, $c_{se,p}$, on the right hand side of (18) can also be considered as the Li-ion concentration on the last outer shell of the solid electrode particle and is given by (8). By the same token, the normalized concentration at the solid-electrolyte interface of the negative electrode, $\varphi_{se,n}$, is given by

$$\varphi_{se,n} = \frac{c_{se,n}}{c_{s,max,n}}. \quad (19)$$

- The difference in the electrolyte potentials of the positive and negative electrodes is given by

$$\phi_{e,p} - \phi_{e,n} = \frac{-I}{2A\kappa^{\text{eff}}}\big(\delta_p + 2\delta_{sep} + \delta_n\big).$$

In a nutshell, the measurement equation in (15) can be rewritten as a function of $\mathbf{c}_s$ and I:

$$\mathbf{V} = h(\mathbf{c}_s, I). \quad (20)$$

The equations (10) and (20) form the state-space model in continuous time.

Converting the State-Space Model from the Continuous-Time domain to a Normalized Discrete-Time Domain

To implement a continuous-time state-space model in a digital computer, it must be converted to a discrete-time state-space model. If the charge/discharge current and voltage measurements are available at distinct time instances, the discrete-time state-space model can be described by the following difference equations:

$$\mathbf{c}_{s,k+1} = \mathbf{F}\mathbf{c}_{s,k} + \mathbf{G}J_k^{Li} \quad (21)$$
$$V_k = h(\mathbf{c}_{s,k}, I_k), \quad (22)$$

where the time index $k = t/\Delta T$, t is the absolute time, and ΔT is the sampling time interval; the system and input matrices are given, respectively, as follows (see Section 1.4. of [20]):

$$\begin{aligned} \mathbf{F} &= \exp(\Delta T \mathbf{A}) \\ \mathbf{G} &= \mathbf{A}^{-1}(\mathbf{F} - \mathbf{I})\mathbf{B}. \end{aligned}$$

Let the normalized concentration vector φ_s be defined as

$$\varphi_s = \frac{\mathbf{c}_s}{c_{s,max}}.$$

Then the normalized discrete-time state-space model can be written as:

$$\varphi_{s,k+1} = \mathbf{F}\varphi_{s,k} + \tilde{\mathbf{G}} J_k^{Li} \quad (23)$$

$$V_k = h(\varphi_{s,k}, I_k), \quad (24)$$

where

$$\tilde{\mathbf{G}} = \mathbf{G}/c_{s,max}.$$

Relationship between Concentrations and SoC

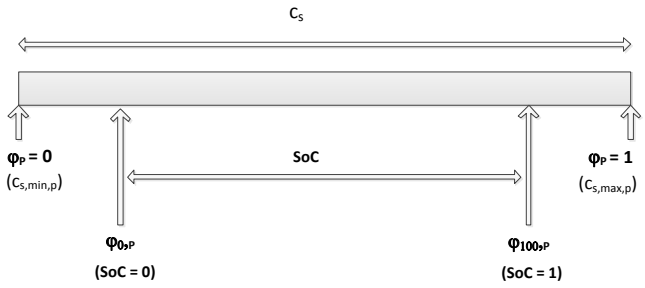

Figure 2: ***Definition of SoC***

The SoC can be defined in many ways. The most common definition is given by the present battery capacity as a percentage of maximum capacity. In this subsection, the SoC is expressed in terms of concentration as described in [7]. Typically, Li-ion cells are designed to be depleted partially or filled up with charge to a level below their maximum capacity. For this reason, the SoC of a cell must be defined within a window of minimum and maximum concentrations (see Fig. 2). For example, the SoC can be defined in terms of the positive electrode, as shown by

$$\text{SoC} = \frac{\varphi_{se,p} - \varphi_{0,p}}{\varphi_{100,p} - \varphi_{0,p}},$$

where $\varphi_{0,p}$ and $\varphi_{100,p}$ denote the normalized concentration in the positive electrode when the cell is fully discharged and charged, respectively, and are empirically determined. The SoC reaches a value of one at the end of complete charge and zero at the end of complete discharge. Given the SoC in terms of the positive electrode, we may find the solid-electrolyte surface concentration in the negative electrode, as shown by

$$c_{se,n} = c_{s,max,n}\varphi_{se,n}, \quad (25)$$

where the normalized solid-electrolyte surface concentration in the negative electrode

$$\varphi_{se,n} = \varphi_{0,n} + \frac{\varphi_{se,p} - \varphi_{0,p}}{(\varphi_{100,p} - \varphi_{0,p})}(\varphi_{100,n} - \varphi_{0,n}).$$

The relationship in (25) is used to estimate the SoC based on a half-cell model because the terminal voltage is a function of both the positive and negative electrode concentrations.

DERIVING THE PST

In the Bayesian estimation framework, the posterior density of the state provides a complete statistical description of the state at that time [3]. On the receipt of a new measurement at time instant k, the Bayesian filter updates the old posterior density of the state in two basic steps:

1. *Time update*, which involves computing the predictive density
2. *Measurement update*, which involves computing the posterior density of the current state

For a linear state-space model with additive Gaussian noise, the Kalman filter is the optimal estimator in a minimum mean squared-error sense. For a nonlinear system however, obtaining a closed from solution to the posterior density is intractable and we have to be content with a suboptimal estimator. In this paper, a suboptimal nonlinear Bayesian estimator is derived in a Gaussian environment. Gaussian densities include two terms, namely, mean and covariance. In the proposed algorithm, the square-root of the various error covariances are propagated over time. The motivation for a square-root formulation is that it always preserve the two basic properties of a covariance matrix, namely, symmetry and positive definiteness. In addition, the square-root algorithms are well known to provide increased stability especially when they are deployed in hardware with limited precision [1].

Time Update

To take into account model mismatches and noisy current measurements, we rewrite the state equation (23) by adding noise as follows:

$$\boxed{\varphi_k = \mathbf{F}\varphi_{k-1} + \tilde{\mathbf{G}} J_{k-1} + \mathbf{w}_k}, \quad (26)$$

where the process noise, $\mathbf{w}_k$, is assumed to be zero-mean Gaussian distributed, i.e., $\mathbf{w}_k \sim \mathcal{N}(\mathbf{0}, \mathbf{Q})$. At the end of this section, we will describe how to find a legitimate value for $\mathbf{Q}$. Given

that $\varphi_{k-1} \sim \mathcal{N}(\hat{\varphi}_{k-1|k-1}, \mathbf{P}_{k-1|k-1})$, we write the predicted state at time k as

$$\hat{\varphi}_{k|k-1} \quad = \quad \mathbb{E}[\varphi_k | V_1, V_2, \dots V_{k-1}], \tag{27}$$

where $\mathbb{E}[.]$ is the expectation operator. Substituting (26) into (27) yields

$$\begin{aligned} \hat{\varphi}_{k|k-1} &= \mathbb{E}[\mathbf{F}\varphi_{k-1} + \tilde{\mathbf{G}}J_{k-1} + \mathbf{w}_k | V_1, V_2, \dots V_{k-1}] \\ &= \mathbf{F}\hat{\varphi}_{k-1|k-1} + \tilde{\mathbf{G}}J_{k-1}. \end{aligned} \tag{28}$$

In deriving (28), we assume that the input J_k has a mean value of $I_k/(A\delta)$ and is independent of battery chemistry. Due to the fact that deriving the predicted state-error covariance is mathematically involved, we first introduce the following notations:

- We shall use $\mathbf{S}_Q$ for square root of the process noise covariance $\mathbf{Q}$.
- A covariance matrix $\mathbf{P}$ can be written in a squared-form, as shown by [1]:

$$\mathbf{P} \quad = \quad \mathbf{S}_o \mathbf{S}_o^T, \tag{29}$$

  where $\mathbf{P} \in \mathbb{R}^{n \times n}$, $\mathbf{S_o} \in \mathbb{R}^{n \times m}$, $m > n$, is a 'fat' matrix. Though $\mathbf{S}_o$ in (29) can be considered as a square-root of $\mathbf{P}$, we prefer to keep the square-root as an $n \times n$ triangular matrix for computational reasons. The transformation of $\mathbf{S}_o$ into a triangular matrix $\mathbf{S}_n \in \mathbb{R}^{n \times n}$ is performed by a triangularization procedure (e.g., Gram-Schmidt based QR-decomposition). When the matrix $\mathbf{S}_o^T$ is decomposed into an orthogonal matrix $\mathbf{V} \in \mathbb{R}^{m \times n}$ and an upper triangular matrix $\mathbf{D} \in \mathbb{R}^{n \times n}$ such that $\mathbf{S}_o^T = \mathbf{V}\mathbf{D}$, we get

$$\mathbf{P} \quad = \quad \mathbf{S}_o \mathbf{S}_o^T = \mathbf{D}^T \mathbf{V}^T \mathbf{V} \mathbf{D} = \mathbf{D}^T \mathbf{D} = \mathbf{S}_n \mathbf{S}_n^T,$$

  where the 'new' square-root of $\mathbf{P}$, $\mathbf{S}_n = \mathbf{D}^T$. In this paper, we simplify matters by using the notation

$$\mathbf{S}_n \quad = \quad \textbf{Tria}(\mathbf{S}_o),$$

  where $\mathbf{S}_o$ is referred to as the 'old' square-root of $\mathbf{P}$.

Now, we write the predicted error covariance

$$\begin{aligned} \mathbf{P}_{k|k-1} &= \text{Cov}[\varphi_k | V_1, V_2, \dots V_{k-1}] \\ &= \text{Cov}[\mathbf{F}\varphi_{k-1} + \tilde{\mathbf{G}}J_{k-1} + \mathbf{w}_k | V_1, V_2, \dots V_{k-1}] \\ &= \mathbf{F}\mathbf{P}_{k|k-1}\mathbf{F}^T + \sigma_j^2 \tilde{\mathbf{G}}\tilde{\mathbf{G}}^T + \mathbf{Q}, \end{aligned} \tag{30}$$

where the variance of the input J_k is assumed to be

$$\sigma_j^2 \quad = \quad \big(\frac{\sigma_i}{A\delta}\big)^2,$$

and σ_i is related to the precision of the current sensor. Using the square-root factor of $\mathbf{Q}$ and manipulating matrices cleverly, we rewrite (30) as

$$\begin{aligned} \mathbf{P}_{k|k-1} &= (\mathbf{F}\mathbf{S}_{k|k-1})(\mathbf{F}\mathbf{S}_{k|k-1})^T + (\sigma_j \tilde{\mathbf{G}})(\sigma_j \tilde{\mathbf{G}})^T + \mathbf{S_Q}\mathbf{S}_Q^T \\ &= [\mathbf{F}\mathbf{S}_{k|k-1} \;\; \sigma_j \tilde{\mathbf{G}} \;\; \mathbf{S}_Q][\mathbf{F}\mathbf{S}_{k|k-1} \;\; \sigma_j \tilde{\mathbf{G}} \;\; \mathbf{S}_Q]^T. \end{aligned}$$

Hence, using the triangularization theory mentioned above, the square-root factor of the predicted state-error covariance can be written as

$$\mathbf{S}_{k|k-1} \quad = \quad \textbf{Tria}([\mathbf{F}\mathbf{S}_{k|k-1} \;\; \sigma_j \tilde{\mathbf{G}} \;\; \mathbf{S}_Q]).$$

Measurement Update Using Potter's Idea

To take into account model mismatches and stochastic factors, similarly to the state equation, we rewrite the measurement equation (24) by adding noise as follows:

$$\boxed{V_k = h(\varphi_{s,k}, I_k) + \mathbf{e}_k}, \tag{31}$$

where the measurement noise, $\mathbf{e}_k$, is assumed to be zero-mean Gaussian distributed, i.e., $\mathbf{e}_k \sim \mathcal{N}(0, \sigma_e^2)$. Typically, the standard deviation of voltage measurement errors, σ_e, can be deduced from the precision of a voltage sensing device. James H. Potter introduced a clever square-root measurement update when the measurement vector is single-dimensional and his algorithm was successfully deployed in the lunar excursion module for the Apollo program half a century ago [5, 12]. Fortunately, in the context of the battery SoC estimation, because the battery terminal voltage measurement is single dimensional, we adapt Potter's idea here to develop the measurement update with little modification.

For completeness, we present the time and measurement update steps of the PST below.

Time Update

1. Assume at time k that the posterior density function $p(\varphi_{k-1}|V_1, V_2, \dots V_{k-1}) = \mathcal{N}(\hat{\varphi}_{k-1|k-1}, P_{k-1|k-1})$ is known. Estimate the predicted state

$$\hat{\varphi}_{k|k-1} \quad = \quad \mathbf{F}\hat{\varphi}_{k-1|k-1} + \tilde{\mathbf{G}}J_{k-1} \tag{32}$$

2. Estimate the square-root factor of the predicted state-error covariance

$$\mathbf{S}_{k|k-1} \quad = \quad \textbf{Tria}\Big([\mathbf{F}\mathbf{S}_{k-1|k-1} \quad \tilde{\mathbf{G}}\sigma_j \quad \mathbf{S}_Q]\Big) \tag{33}$$

Measurement Update

1. Calculate the vector

$$\mathbf{T}_k \quad = \quad \mathbf{S}_{k|k-1}^T \mathbf{H}_k^T, \tag{34}$$

   where $\mathbf{H}$ is the Jacobian of $h(.)$ estimated at $\hat{\varphi}_{k|k-1}$.

2. Calculate the scalar

$$\alpha_k \quad = \quad \frac{1}{\mathbf{T}_k^T \mathbf{T}_k + \sigma_e^2} \tag{35}$$

3. Estimate the filter gain

$$\mathbf{W}_k \quad = \quad \alpha_k \mathbf{S}_{k|k-1} \mathbf{T}_k \tag{36}$$

4. Estimate the predicted measurement

$$\hat{V}_{k|k-1} \quad = \quad h(\hat{\varphi}_{k|k-1}, I_k) \tag{37}$$

5. Estimate the updated state

$$\hat{\varphi}_{k|k} \quad = \quad \hat{\varphi}_{k|k-1} + \mathbf{W}_k (V_k - \hat{V}_{k|k-1}) \tag{38}$$

6. Calculate the scalar

$$\gamma_k \quad = \quad \frac{1}{1 + \sigma_e \sqrt{\alpha_k}} \tag{39}$$

7. Estimate the square-root factor of the updated state-error covariance

$$\mathbf{S}_{k|k} \quad = \quad \mathbf{S}_{k|k-1} - \gamma_k \mathbf{G}_k \mathbf{T}_k^T \tag{40}$$

Note: Unlike the regular/unnormalized state-space model, the normalized one does not require laborious tuning or *a priori* knowledge for setting up various state-space model parameters, e.g.,

- *How do we determine a suitable value for process-noise covariance* $\mathbf{Q}$? Because the $i-$th state variable, $\varphi_{s_i,k}$, refers to a normalized concentration in the i-th shell of the solid particle, we may expect the squared-error in the estimate to lie within the following constraint:

  $$0 \leq (\hat{\varphi}_{s_i,k|k} - \varphi_{s_i,k})^2 \quad \leq \quad 1, \quad \forall i,k$$

  This implies that a logical choice for $\mathbf{Q}$ is the identity matrix.

- *What are the legitimate values of* $\hat{\varphi}_{s,1|0}$ *and* $\mathbf{P}_{1|0}$*, to initialize an estimator*? An obvious choice for $\hat{\varphi}_{s_i,1|0}$ is 0.5, because it lies in the middle of its two extreme values. In this case, all the diagonal entries of the initial estimation error covariance lie within the following constraint:

  $$0 \leq \mathbf{P}_{1|0}[i,i] \quad \leq \quad 0.25, \quad \forall i$$

  Therefore, a legitimate choice for $\mathbf{P}_{1|0}$ is $0.25\mathbf{I}$, where $\mathbf{I}$ is the identity matrix.

COMPUTER EXPERIMENTS

In this section, we assess the effectiveness of the proposed approach and compare it with the method described by Domenico *et al*. in [7]. To make matters clear, the proposed approach in this paper was named the PST/nECM (Potter SoC tracker using the normalized electrochemical state-space model) while Domenico *et al.*'s method was named the EKF/ECM (Extended Kalman Filter using the unnormalized electrochemical state-space model). The process and measurement noise covariances for the PST/nECM were set to be $\mathbf{Q} = \mathbf{I}$ and $\sigma_e^2 = 10^{-4}$, respectively, (see Section (DERIVING THE PST)), whereas for the EKF/ECM, $\mathbf{Q}$ and σ_e^2 were obtained through optimization and set to be $\mathbf{Q} = 12\mathbf{I}$ and $\sigma_e^2 = 10$, respectively (see Section IV of [7]). To initialize both estimators, we assumed the initial SoC to be 0.5. For a fair comparison, we performed several simulations using different current demand profiles as described below.

In the first experiment, we considered a current profile from the FreedomCAR operational manual [9]. The FreedomCAR profile consists of a 30A current discharge for 18s, rest for 32s, 22.5A charge for 10s followed by rest (see Fig. 3). One of the reasons for choosing this profile is that it reveals effects attributable to solid diffusion during pulse operations of HEV batteries. The measurement noise statistic was assumed to be zero-mean Gaussian with a standard deviation of 1 mV. The reference Li-ion cell data were generated by spatially discretizing the electrochemical model of 200 shells in total (for both the positive and negative electrodes) as described in Section DERIVING THE PS), and sampling at a rate of 10Hz. The initial SoC was set to be 0.65. For SoC estimation estimation, the electrochemical model for the positive electrode (half-cell model) was considered. Moreover, spatial discretization of three shells was found to be sufficient to capture this half-cell model.

As shown in Figs. 4 and 5, the EKF/ECM and PST/nECM performed almost identically in estimating the SoC and the voltage . However, they deviated substantially in their confidence on estimates (see Fig. 4)– the PST/nECM yields a reasonable value for the 99% confidence band around its voltage estimate, whereas it is highly broad in the case of the EKF/ECM implying that the EKF/ECM is overly pessimistic about its voltage estimate. This aspect of the EKF/ECM is undesirable in many situations. To illustrate this, we considered a scenario where outlier measurements were present.

We generated outlier measurements by introducing zero readings deliberately at random time instants. Both the EKF/ECM and PST/nECM used the outlier detection method as described in Appendix B in their measurement updates. As shown in Figs. 6 and 7, the PST/nECM seems to be robust to outliers whereas the EKF/ECM does not. The EKF/ECM starts to diverge as soon as it encounters an outlier despite the inclusion of the outlier detection method. It seems to be incapable of discerning good measurements from outliers because of its unduly pessimistic confidence band. But, the PST is able to detect outliers, exclude them, and survive mainly because of its reasonable parameter usage (see Fig 8 for evidence). For a fair comparison, we ran the experiment for 100 independent Mote Carlo runs. The PST/nECM survived in all the runs successfully whereas the EKF/ECM failed in all of them.

Motivated by these results, we applied the PST/nECM to a series of pulsed discharge current demand profile. Fig. 10 shows the current profile in which 10A discharge current for a period of 25s, followed by 75s-long open-circuit relaxation was applied in a periodic fashion. As can be seen from Figs. 11 and 12, the PST/nECM estimates the SoC accurately even in the presence of outlier measurements, validating the virtue of estimating the second-order statistics accurately.

CONCLUDING REMARKS

In this paper, we presented a square-root algorithm called the Potter SoC Tracker (PST) to estimate the SoC accurately and reliably. For estimation, we derived a normalized electrochemical state-space model based on Li-ion chemistry. For computational reasons, we reduced the diffusion model to a relatively less order single-electrode model and normalized with respect to the maximum Li-ion concentration. It was successfully demonstrated that the PST using this normalized state-space model estimated the SoC with an accuracy above 95% when applied to a highly challenging FreedomCAR current profile and a pulse current test with outlier voltage measurements. This accuracy rate is acceptable for battery management/control applications. A couple of future interesting research topics are in order: (i) To investigate controllability and observability of the electrochemical state-space model and their implications (ii) To track various electrochemical model parameters and adaptively include them to ensure that the electrochemical state-space is sufficiently accurate over the entire lifespan of a battery.

REFERENCES

[1] Arasaratnam, I., Haykin, S., and Hurd, T., "Cubature Kalman Filtering for Continuous-Discrete Systems: Theory and Simulations," *IEEE Trans. Signal Processing*, 58(10), pp. 4977-4993, Oct. 2010.

[2] Bard, AJ., and Faulkner, LR., "Electrochemical Methods: Fundamentals and Applications," *Russian J. Electrochemistry*, Vol. 38, 2002.

[3] Bar Shalom, Y., Li, X. R. and Kirubarajan, T., *Estimation with Applications to Tracking and Navigation*, NY: Wiley & Sons, 2001.

[4] Blood, Paul J., and Sotiropoulos, S., "An electrochemical technique for state of charge (SOC) probing of positive leadacid battery plates." *J. power sources*, vol. 110, no. 1, 2002.

[5] Born, GH., "Potter Square Root Filter", ASEN 5070 Course Handout, University of Colorado at Boulder, `http://ccar.colorado.edu/ASEN5070/handouts.htm`, viewed Sept. 16, 2012.

[6] Buchmann, I., "Does the Battery Fuel Gauge Lie? Why the Battery State-of-charge cannot be measured accurately," `http://www.buchmann.ca`, Viewed Sept. 2012.

[7] Domenico, D., Giovanni, F., and Stefanopoulou, A., "Lithium-ion battery state of charge estimation with a Kalman filter based on an electrochemical model," *IEEE Int'l Conf. in Control Applications*, CCA 2008.

[8] Doyle, M., Fuller, T., Newman, J., "Modeling of galvanostatic charge and discharge of the lithium/polymer/insertion cell," *J. Electrochemical Soc.* , vol. 140, pp. 1526-1533, 1993.

[9] Freedomcar battery test manual for power-assist hybrid elecric veicles, *DOE/ID-11069*, 2003.

[10] Charkhgard, M., and Farrokhi M., "State-of-Charge Estimation for Lithium-Ion Batteries Using Neural Networks and EKF," *IEEE Trans. Industrial Electronics*, Vol. 57, 2010.

[11] Fuller, T., Doyle, M., and Newman, J., "Simulation and optimization of the dual lithium ion insertion cell," , *J. Electrochemical Soc.*, vol. 141, pp. 1-10, 1994.

[12] Grewal, MS., & Andrews, AP., *Kalman Filtering Theory and Practice Using MATLAB*, Third Edition, Wiley & Sons, 2008.

[13] Hsieh, GC., Chen, LR., and Huang, KS., "Fuzzy-controlled li-ion battery charge system with active state-of-charge controller," *IEEE Trans. Ind. Electron.*, Vol. vol. 48, pp. 585593, 2001.

[14] Huet, F., "A review of impedance measurements for determination of state- of-charge or state-of-health of secondary batteries," *J. Power Sources*, Vols. vol. 70, no. 1, pp. 5969, 1998.

[15] Hu, X., Li, S., Peng, H., "A comparative study of equivalent circuit models for Li-ion batteries" *J. Power Sources*, pp. 39213932, 2011.

[16] Newman, J., and Tiedemann, W., "Porous-electrode theory with battery applications," *AIChE Journal*, Vol. 21, pp. 25-41, 1975.

[17] Pattipati, B., Sankavaram, C., Pattipati, KR., "System Identification and estimation framework for pivotal automotive battery management system charateristics", *IEEE Trans. Syst. Man Cybern*, pp. 869884, 2011.

[18] Plett, G., "Extended Kalman filtering for battery management systems of LiPB-based HEV battery packs," *J. Power Sources*, pp. 252261, 2004.

[19] Pop, V., Bergveld, HJ., het Veld, JO., Regtien, PL., Danilov, D., & Notten, PL, "Modeling battery behavior foraccurate state-of-charge indication," *J. Electrochem. Soc.*, 2006

[20] Simon, D., *Optimal State Estimation:Kalman, H_∞, and Nonlinear Approaches*, Wiley, 2006.

[21] Smith, K. and Wang, CY., "Solid-state diffusion limitations on pulse operation of a lithium-ion cell for hybrid electric vehicles", *J. Power Sources*, 161:628639, 2006.

[22] Tarascon, JM. and Guyomard, D., "Li Metal-Free Rechargeable Batteries Based on Li+xMn2O4 Cathodes (0 x 1) and Carbon Anodes", *J. Electrochemical Society*, Vol. 138, pp. 2864-2868, 1991.

[23] Verbrugge, MW., and Koch, BJ., "Electrochemical analysis of lithiated graphite anodes", *J. Electrochem. Soc.*, 150, 2003.

[24] Verbrugge, MW, and Tate, E., "Adaptive state of charge algorithm for nickel metal hydride batteries including hysteresis phenomena", *J. Power Sources*, pp. 236249, 2004.

[25] Wang, CY., Gu, WB., and Liaw, BY., "Micro-Macroscopic Coupled Modeling of Batteries and Fuel Cells Part:I . Model Development.", *J. Electrochemical Society*, vol. 145, no. 10, 1998.

[26] Wei, KX., and Chen, QY., "Battery SOC Estimation based on Multi-model Adaptive Kalman Filter," *Advanced Materials Research*, pp. 2211-2215, 2012.

APPENDIX A: OUTLIER DETECTION

Outlier measurements can be caused by various engineering problems such as discontinuities from hardware switching in digital systems, sensor faults, strong electro-magnetic interference and co-channel interference. Outliers are known to influence an estimator strongly. They cause the estimator to drift towards them quickly leading to a catastrophic failure. Unless a corrective action is taken to eliminate the outliers, the estimator may stop to run after throwing out an error message. In this subsection, a simple outlier detection method using a statistical distance measure is presented [3]. To simplify matters, consider a linear measurement model with additive Gaussian noise, as shown by

$$\mathbf{y}_k \quad = \quad \mathbf{H}\mathbf{x}_k + \mathbf{e}_k,$$

where the measurement noise is assumed to be zero mean Gaussian, $\mathbf{e}_k \sim \mathcal{N}(\mathbf{0}, \mathbf{R})$. Given $\mathbf{x}_{k-1} \sim \mathcal{N}(\hat{\mathbf{x}}_{k-1|k-1}, \mathbf{P}_{k-1|k-1})$, the the normalized-innovations (predicted-measurement error) squared can be proved to be chi-squared distributed, as shown by [3]:

$$(\mathbf{y}_k - \hat{\mathbf{y}}_{k|k-1})^T \mathbf{P}^{-1}_{\mathbf{y},k|k-1} (\mathbf{y}_k - \hat{\mathbf{y}}_{k|k-1}) \quad \sim \quad \chi^2_{n,\alpha}, \quad (41)$$

where n is the degree of freedom and equals to the dimension of the measurement vector, α is the confidence level and the innovations covariance $\mathbf{P}_{\mathbf{y},k|k-1} = (\mathbf{H}\mathbf{P}_{k-1|k-1}\mathbf{H}^T + \mathbf{R})$. When the current measurement fails to satisfy (41), it can be declared as an outlier and excluded from subsequent computations. For the SoC estimation case, a voltage measurement can be declared as an outlier with a confidence of 95% when the normalized-innovations squared exceeds $\chi^2_{1,95\%} = 3.84$. In this case, the estimator rejects the outlier measurement and the updated-state statistics simply become the predicted-state statistics. In the following section, we will demonstrate how the PST using this idea succeeds to survive in an environment with outliers.

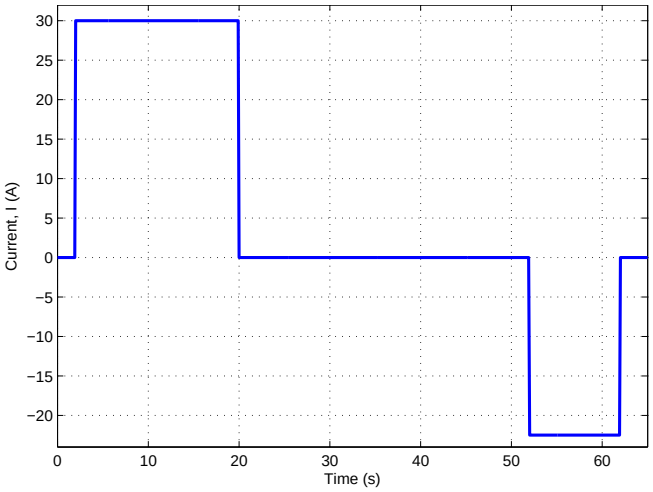

Figure 3: ***FreedomCAR Current Profile***

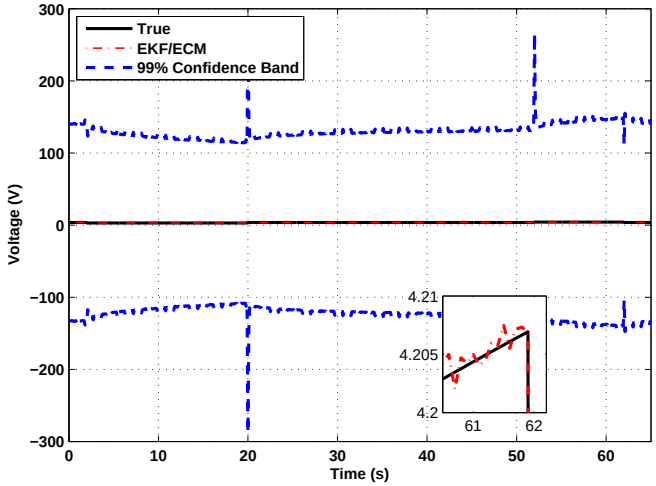

(a)

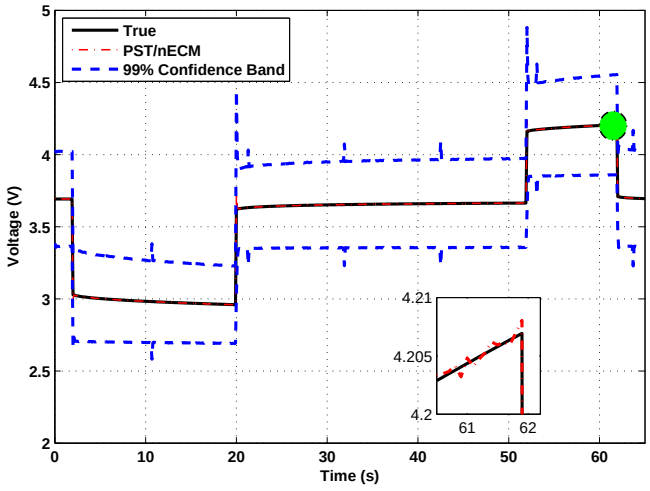

(b)

Figure 4: ***Case (I): Voltage Estimation without Outlier Measurements***

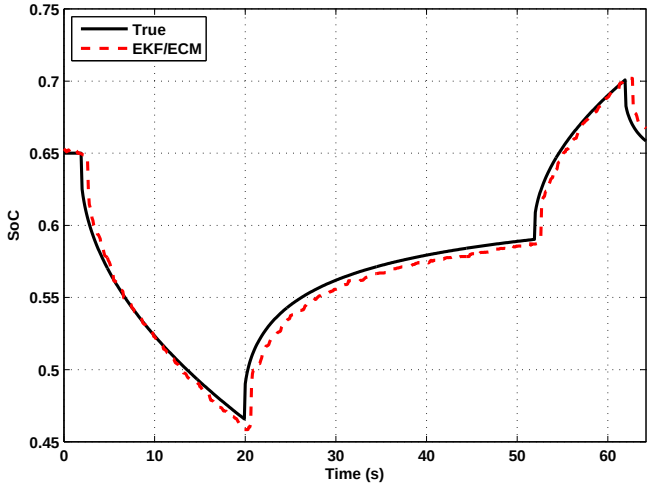

(a)

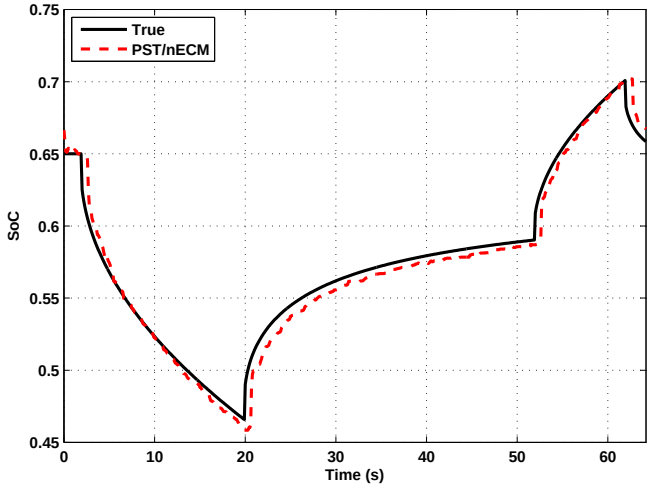

(b)

Figure 5: ***Case (I): SoC Estimation without Outlier Measurements***

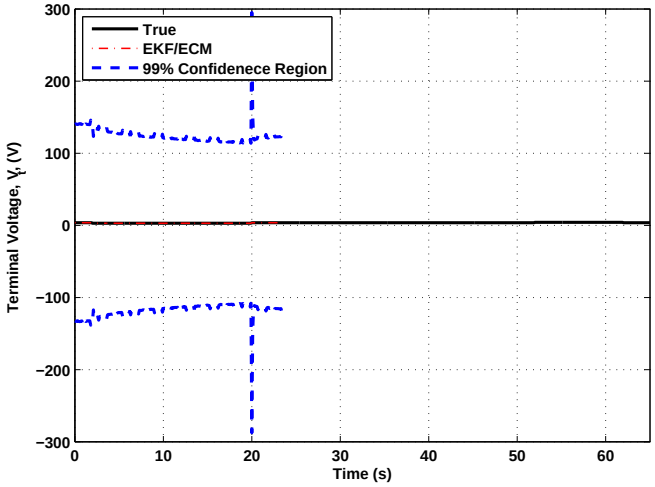

(a)

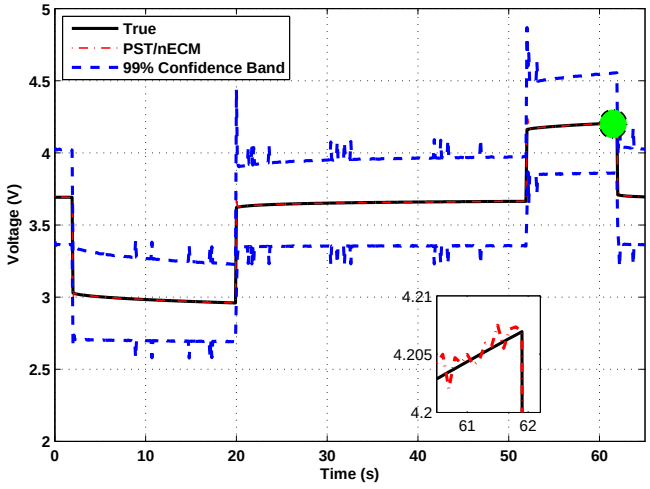

(b)

Figure 6: ***Case II: Voltage Estimation with Outlier Measurements***

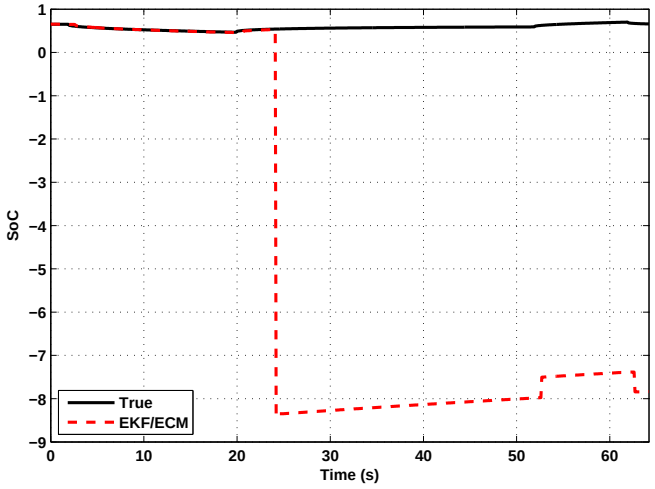

(a)

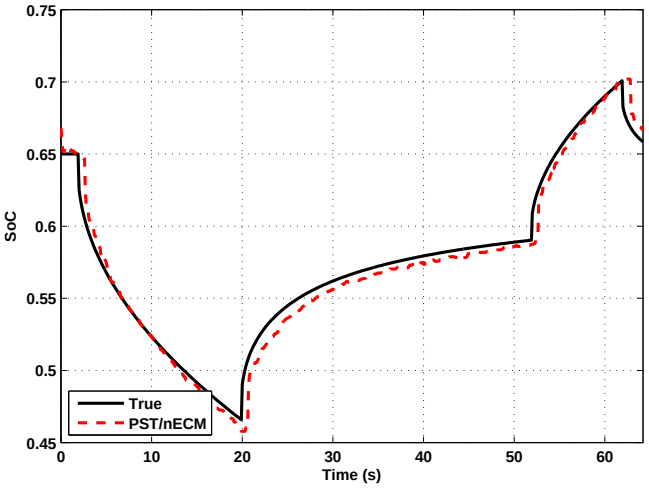

(b)

Figure 7: ***Case II: SoC Estimation with Outlier Measurements***

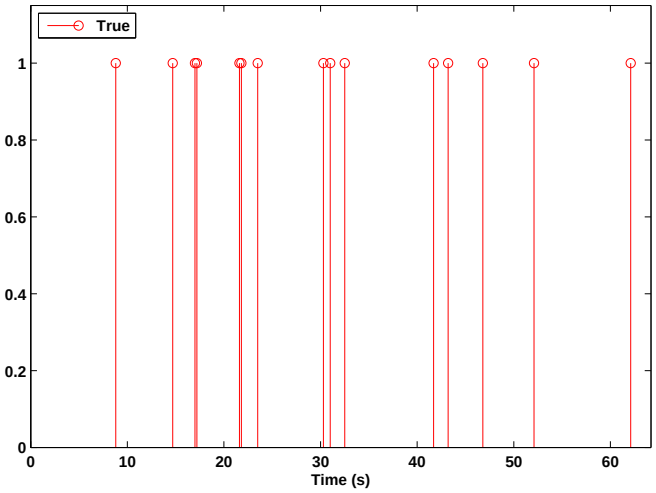

(a) Time Instances where Outliers Were Present

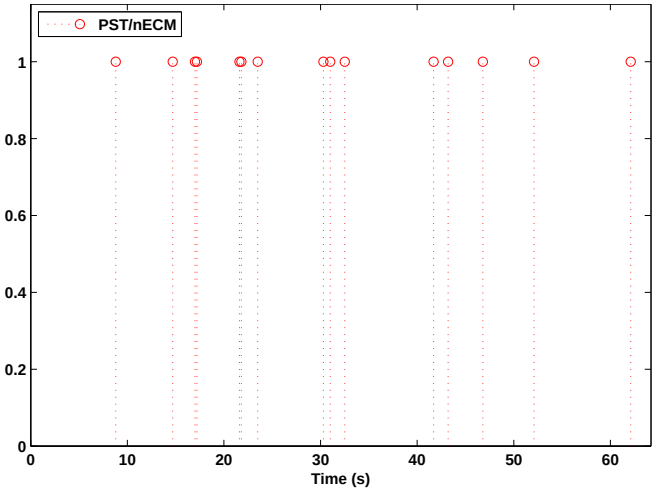

(b) Outliers Detected by PST/nECM

Figure 8:

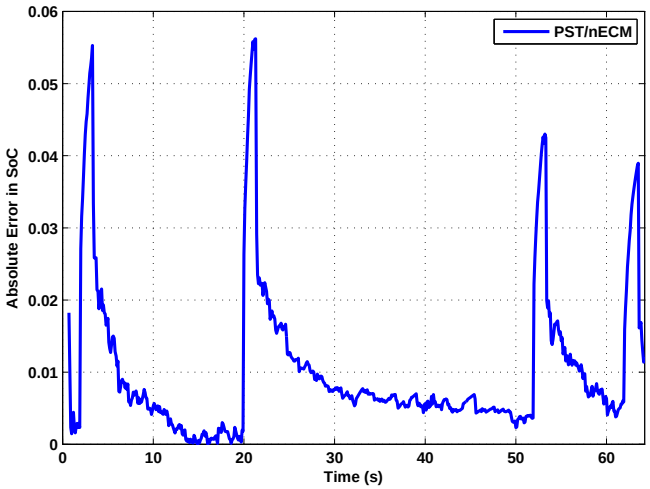

Figure 9: ***Absolute Error in Soc Estimation***

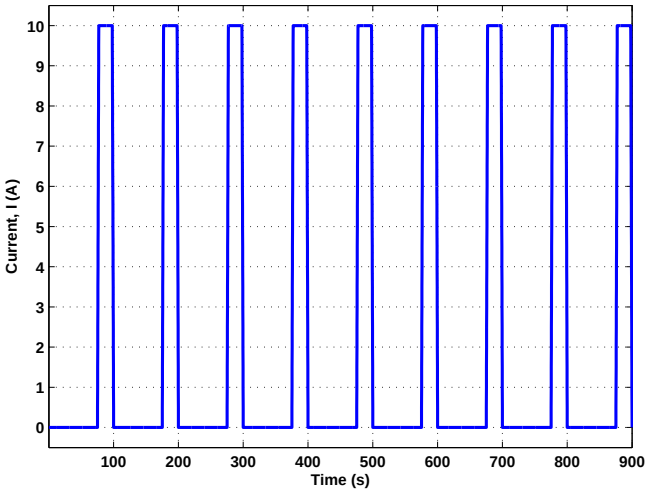

Figure 10: ***Pulse Discharge Current Profile***

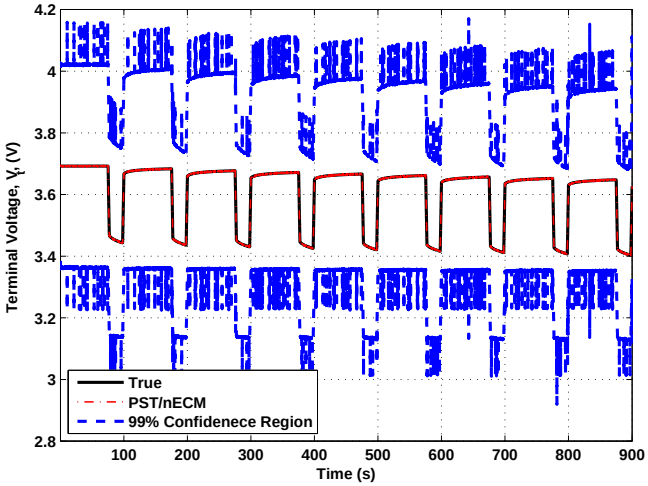

Figure 11: ***PST/nECM: Voltage Estimation***

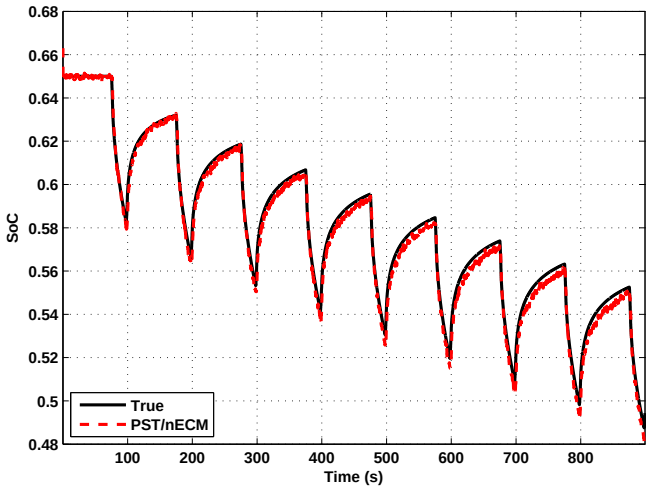

(a) PST/nECM: SoC Estimation with Outliers

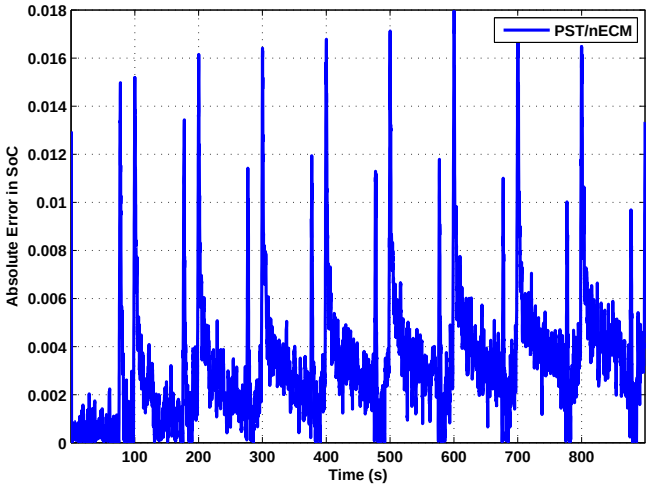

(b) PST/nECM: SoC Estimation Error

Figure 12:

Table 1: ***Li-Ion Cell Parameters– Anode consists of graphite whereas cathode is $LiCoO_2$***

Name	Symbol	Unit	Negative Electrode	Separator	Positive Electrode
Thickness	δ	cm	50×10^{-4}	50×10^{-4}	50×10^{-4}
Electrode plate area	A	cm^2	10452	10452	10452
Particle radius	R_s	cm	1×10^{-4}		50×10^{-4}
Active material volume fraction	ε_s		0.580		0.5
Porosity	ε_e		0.332	0.5	0.330
Conductivity of solid active material	σ	$\Omega^{-1}cm^{-1}$	1		0.1
Effective conductivity of solid active material	σ^{eff}		$\varepsilon_s\sigma$		$\varepsilon_s\sigma$
Solid phase diffusion coefficient	D_s	cm^2s^{-1}	2.0×10^{-12}		3.7×10^{-12}
Maximum solid phase concentration	$c_{s,\text{max}}$	molcm^{-3}	16.1×10^{-3}		16.1×10^{-3}
Transference number	t^0		0.363	0.363	0.363
Electrolyte phase ionic conductivity	κ	$\Omega^{-1}cm^{-1}$	$0.0158c_e\times$ $\exp(0.85c_e^{1.4})$	$0.0158c_e\times$ $\exp(0.85c_e^{1.4})$	$0.0158c_e\times$ $\exp(0.85c_e^{1.4})$
Effective electrolyte phase ionic conductivity	κ^{eff}		$\varepsilon_e^{1.5}\kappa$	$\varepsilon_e^{1.5}\kappa$	$\varepsilon_e^{1.5}\kappa$
Effective electrolyte phase diffusion conductivity	κ_D^{eff}		$\frac{2RT\kappa_{\text{eff}}(t_+^0-1)}{F}$	$\frac{2RT\kappa_{\text{eff}}(t_+^0-1)}{F}$	$\frac{2RT\kappa_{\text{eff}}(t_+^0-1)}{F}$
Electrolyte phase diffusion coefficient	D_e	cm^2s^{-1}	2.6×10^{-6}	2.6×10^{-6}	2.6×10^{-6}
Effective electrolyte phase diffusion coefficient	D_e^{eff}		$\varepsilon_e^{1.5}D_e$	$\varepsilon_e^{1.5}D_e$	$\varepsilon_e^{1.5}D_e$
Average electrolyte concentration	$\bar{c}_e$	molcm^{-3}	1.2×10^{-3}	1.2×10^{-3}	1.2×10^{-3}
Anodic & cathodic transfer coefficients	α_a, α_c		0.5,0.5		0.5,0.5
Active surface area per electrode unit volume	a_s	cm^{-1}	$\frac{3\varepsilon_e}{R_s}$		$\frac{3\varepsilon_e}{R_s}$
Film resistance at electrode surface	R_f	$m\Omega$	20		20